# Effect of stacking faults on the photoluminescence spectrum of zincblende GaN

S. A. Church,[1] S. Hammersley,[1] P. W. Mitchell,[1] M. J. Kappers,[2] L. Y. Lee,[2] F. Massabuau,[2] S. L. Sahonta,[2] M. Frentrup,[2] L. J. Shaw,[3] D. J. Wallis,[2,4] C. J. Humphreys,[2] R. A. Oliver,[2] D. J. Binks,[1] and P. Dawson[1]

[1]*School of Physics and Astronomy, Photon Science Institute, University of Manchester, Manchester M13 9PL, United Kingdom*

[2]*Department of Materials Science and Metallurgy, University of Cambridge, 27 Charles Babbage Road, Cambridge CB3 0FS, United Kingdom*

[3]*Anvil Semiconductors Ltd., Future Business Centre, King's Hedges Road, Cambridge CB4 2HY, United Kingdom*

[4]*Centre for High Frequency Engineering, University of Cardiff, 5 The Parade, Newport Road, Cardiff CF24 3AA, United Kingdom*

(Received 17 February 2018; accepted 23 April 2018; published online 10 May 2018)

The photoluminescence spectra of a zincblende GaN epilayer grown via metal-organic chemical vapour deposition upon 3C-SiC/Si (001) substrates were investigated. Of particular interest was a broad emission band centered at 3.4 eV, with a FWHM of 200 meV, which extends above the bandgap of both zincblende and wurtzite GaN. Photoluminescence excitation measurements show that this band is associated with an absorption edge centered at 3.6 eV. Photoluminescence time decays for the band are monoexponential, with lifetimes that reduce from 0.67 ns to 0.15 ns as the recombination energy increases. TEM measurements show no evidence of wurtzite GaN inclusions which are typically used to explain emission in this energy range. However, dense stacking fault bunches are present in the epilayers. A model for the band alignment at the stacking faults was developed to explain this emission band, showing how both electrons and holes can be confined adjacent to stacking faults. Different stacking fault separations can change the carrier confinement energies sufficiently to explain the width of the emission band, and change the carrier wavefunction overlap to account for the variation in decay time. *Published by AIP Publishing.*
https://doi.org/10.1063/1.5026267

## I. INTRODUCTION

Commercial GaN-based white LEDs typically contain a blue emitter which consists of multiple InGaN/GaN quantum wells (QWs) grown on c-plane wurtzite (wz) GaN. Carriers in these wells recombine to produce blue light with internal quantum efficiencies reaching 90%.[1] Combining the output of these blue LEDs with that of a yellow phosphor results in a light source which appears white and is therefore suitable for many lighting applications. However, the conversion efficiency of the phosphor limits the efficiency of the device at low drive currents. An attractive alternative would be to colour-mix the emission from separate red, green, and blue LEDs to create the white light. This would both avoid the need for a phosphor and allow colour-tuneability of the source. Efficient red LEDs are produced using alloys of InGaAsP.[2] However, green LEDs use InGaN/GaN QWs that are significantly less efficient than their blue counterparts. A greater indium content is required within the QWs to achieve green emission, which increases the electric field across the QW. This is believed to reduce the spatial overlap of the carriers and thereby increase the radiative lifetime and reduce the efficiency.[3]

It is proposed that these effects can be ameliorated by growing QW structures with a reduced electric field. This can be achieved via growth on the nonpolar a-[4–6] and m-[7,8] planes, or growth on semipolar planes[9,10] of wz-GaN. Alternatively, GaN can be grown in the [001] direction of the zincblende (zb) crystal phase, which has increased symmetry when compared to wz-GaN, resulting in zero polarisation field across the QWs.[11] Heteroepitaxial growth of zb-GaN can be performed upon 3C-SiC/Si (001) substrates,[12–20] which offers the advantages of being commercially viable and having a relatively small lattice mismatch of 3.7% with GaN.[21]

However, growing phase-pure zb-GaN is challenging with epilayers often containing wz-GaN, as either stacking faults (SFs) or crystal inclusions, which has been reported to reduce the radiative efficiency of zb-GaN based QW structures.[22] The phase purity and structural quality of the zb-GaN can be assessed via X-ray diffraction (XRD),[23–26] Raman spectroscopy,[23,24] and high-resolution transmission electron microscopy (HR-TEM).[16,27,28] The presence of wz-GaN in zb-GaN epilayers has been seen to result in narrow peaks or a broad emission band in the low temperature photoluminescence (PL) spectrum at energies between the bandgaps of zb and wz-GaN.[12–14,18,24,29] A recent work on a sample of zb-GaN grown on 3C-SiC reported the observation of a broad emission that encompasses the bandgaps of zb and wz-GaN and extends as far as 3.6 eV. It was suggested that carrier confinement around a high density of SFs was responsible for the band.[20]

In this paper, we report further investigations into the nature of the high energy emission band (HEB) in zb-GaN epilayers via an investigation of the luminescence of an epilayer grown using metal-organic chemical vapour deposition (MOCVD) onto the 3C-SiC/Si (001) substrates. A model for the band alignment adjacent to SFs is developed to explain the origin of the HEB.

## II. EXPERIMENT

A zb-GaN epilayer was grown using MOCVD on a $1 \times 1$ in.$^2$ piece of a 100 mm diameter substrate consisting of 7 $\mu$m of 3C-SiC upon 750 $\mu$m of Si (001). The GaN growth conditions were similar to those described for sample A in Ref. 20 but grown to a greater thickness of 650 nm. The film was Si-doped to $5 \times 10^{18}$ cm$^{-3}$.

The SF density and the spacing between SFs were determined by TEM imaging of the sample. A JEOL 4000 EX operated at 400 kV was used for bright-field (BF) TEM imaging, while a Tecnai F20 operated at 200 kV was used for HR-TEM in addition to the JEOL 4000 EX. Diffraction patterns from the TEM and HR-TEM showed no evidence of large wz-GaN inclusions. BF imaging indicated that there is a significant number of SFs distributed in a non-uniform manner, as shown in Fig. 1. There are regions without SFs (up to 340 nm along [110]), and SF bunches, within which the SF separations are between 0.8 and 77 nm, which is clearly shown by a combination of BF and HR-TEM imaging.

The SF densities for the sample were obtained from BF imaging of SF bunches, as in Fig. 1, at 100 nm from the epilayer surface. The SF densities across two 1 $\mu$m lines along [110] are $0.9 \times 10^5$ cm$^{-1}$ and $2.2 \times 10^5$ cm$^{-1}$. However, such SF densities are underestimates, since BF imaging is not able to resolve SFs separated by less than 7 nm. From HR-TEM measurements, around 20% of SFs are separated by less than 7 nm.

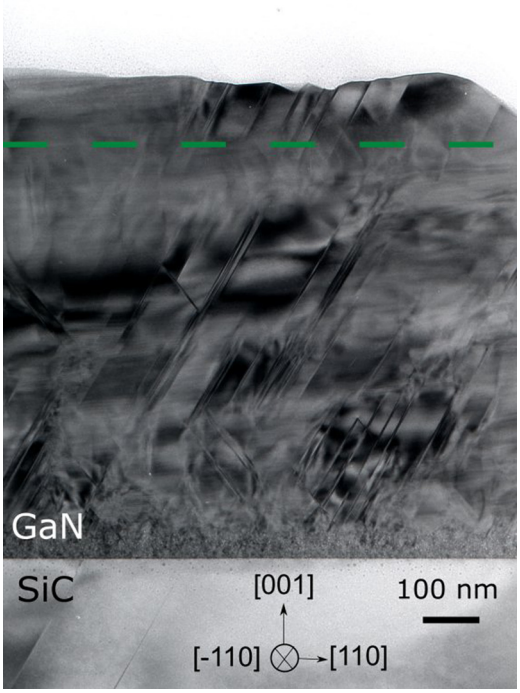


FIG. 1. Bright field TEM image of the zb-GaN epilayer (g = 002, zone axis = [−110]). The SF density was measured at the green dashed line, approximately 100 nm below the epilayer surface, to be $2.2 \times 10^5$ cm$^{-1}$.

XRD reciprocal space maps of the $113_{zb}$ and $1\text{-}103_{wz}$ GaN reflections were taken using a PANalytical Empyrean diffractometer equipped with a two-bounce hybrid monochromator, 1/4° primary beam slit, and a PIXcel solid-state area detector. For phase analysis, the intensity profile along the SF-streak between both reflections (Q||[111]) was extracted and is shown in Fig. 2. Pseudo-Voigt fits of the $113_{zb}$ and $1\text{–}103_{wz}$ GaN reflections at about their theoretical position of 4.03 Å and 3.65 Å, respectively, revealed a phase purity of 85% zb-GaN and 7.5% wz inclusions. A third Pseudo-Voigt fit in between both reflections revealed the presence of 7.5% highly defective zb-GaN in the epilayer.

PL spectra were measured with the sample mounted on the cold finger of a temperature controlled closed-cycle helium cryostat and excited with a continuous-wave He-Cd laser emitting at 325 nm. The excitation beam was modulated with an optical chopper and focussed to give a maximum power density of 4000 W cm$^{-2}$. PL-excitation (PLE) spectroscopy was performed using a 300 W Xe lamp and a monochromator to provide a source with a variable wavelength and a power density of $\approx 0.4$ mW cm$^{-2}$. The luminescence was detected using a GaAs photomultiplier tube coupled to a double-grating spectrometer with a resolution of 24 Å and a lock-in amplifier, synchronised to the chopper. A longpass filter was included at the entrance slit to the spectrometer to eliminate the scattered laser light.

A frequency-tripled Ti:Sapphire laser producing 100 fs pulses at a final wavelength of 267 nm was used to excite the sample for time-resolved PL studies, resulting in an estimated injected carrier density of $3 \times 10^{12}$ cm$^{-2}$. The PL decay transients were measured using the time-correlated single-photon counting technique.

## III. RESULTS AND DISCUSSION

### A. Experimental results

The PL spectrum of the sample was measured for temperatures between 10 K and 300 K, as shown in Fig. 3. The

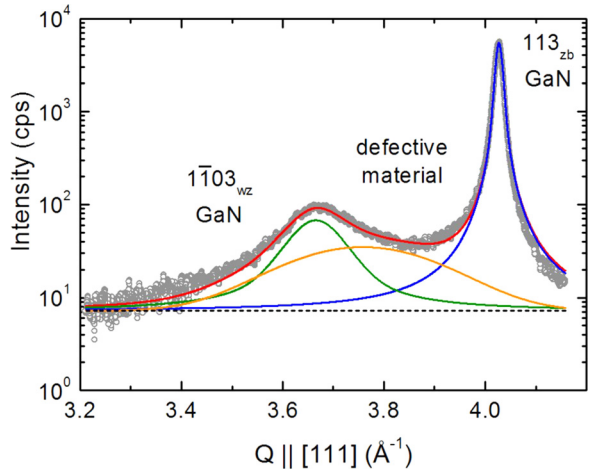


FIG. 2. XRD intensity profile along the [111] SF streak through the $1\text{-}103_{wz}$ and $113_{zb}$ reflections (grey circles). The integrated intensity of Pseudo-Voigt fits for the wz phase (green), zb phase (blue), and defective zb GaN material (orange) was used to estimate the phase portions.

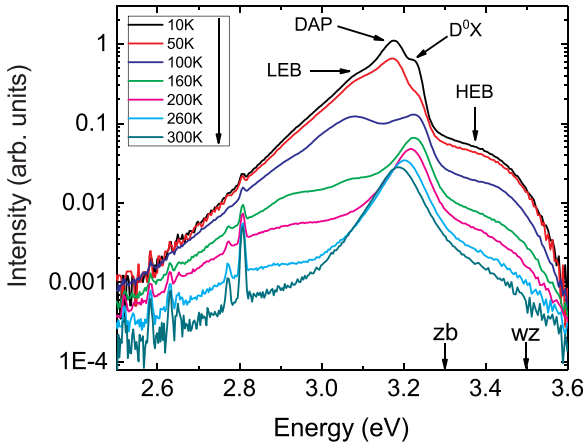


FIG. 3. Temperature dependent PL spectra for the sample under CW excitation with a 325 nm He-Cd laser and a power density of 10 W $cm^{-2}$. Sharp peaks at 2.81 eV and 2.77 eV are laser plasma lines. The nominal bandgaps of zb (3.3 eV) and wz-GaN (3.5 eV) are indicated on the energy axis.[30]

spectrum at 10 K exhibits emission peaks at 3.225 eV and 3.175 eV, along with a low energy band (LEB) at energies below 3.1 eV and an HEB with a peak energy around 3.4 eV.

The 10 K peak at 3.225 eV is due to recombination of donor-bound excitons ($D^0X$).[18] This peak is attributed to free-excitons at temperatures above 160 K, and redshifts due to bandgap shrinkage. The peak at 3.175 eV quenches rapidly with temperature such that it is unresolvable by 100 K, and power dependent PL measurements show that the peak blueshifts by 20 meV as the excitation power is increased by 3 orders of magnitude. This peak is therefore attributed to donor-acceptor pair (DAP) recombination.[31] The LEB consists of several features which quench with temperature at different rates, resulting in the emergence of other peaks around 160 K. Such a band has been observed previously[17,31,32] and has been attributed to a mixture of DAP and free-to-bound transitions, and associated phonon replicas.

The HEB is of particular interest since it extends above the bandgap of zb-GaN (3.3 eV) and wz-GaN (3.5 eV) at 10 K. The shape of the HEB can vary with excitation position on the epilayer, but the peak energy is typically around 3.4 eV and the FWHM is around 200 meV. Emission in this region of the spectrum has been attributed to inclusions of wz-GaN in the epilayer.[12–14,18,24,29]

PLE spectra were recorded, at 10 K, by varying the excitation photon energy while maintaining a constant detection photon energy, and are shown in Fig. 4. These spectra show that the intensity of the DAP emission reduces as the excitation energy is reduced below approximately 3.3 eV. This absorption edge is caused by a reduction in the joint density of states for the absorbing states. The absorption edge corresponds well with the bandgap of zb-GaN, indicating that the DAP emission is due to recombination of carriers in zb-GaN. In contrast, the HEB is associated with an absorption edge around 3.7 eV and a relatively large (≈200 meV) energy shift between absorption and emission. This absorption edge does not correspond with the bandgap energies of zb- or wz-GaN and suggests that the HEB is not due to recombination in large wz-GaN inclusions, where we would see an absorption

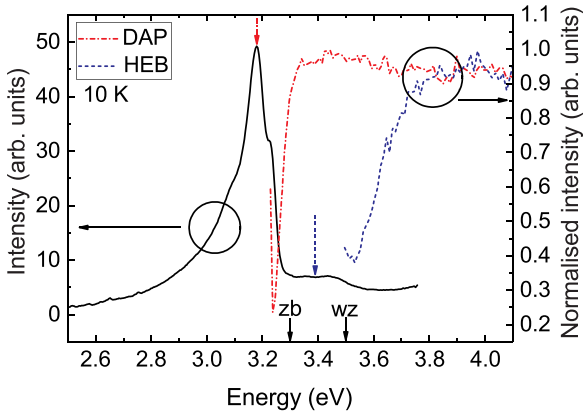


FIG. 4. PLE spectra measured at 10 K with excitation from a Xe lamp. The red dotted line corresponds to a detection energy of 3.18 eV, indicated by the red dotted arrow on the DAP peak. The blue dotted line is at a detection energy of 3.39 eV, shown by the blue dotted arrow on the HEB (blue). The PL spectrum obtained, with excitation at 4.1 eV, under the same conditions is also shown for reference (black). The nominal bandgaps of zb (3.3 eV) and wz-GaN (3.5 eV) are indicated on the energy axis.[30]

edge similar to bulk wz-GaN with a sharp absorption edge around 3.5 eV.[33] This is further supported by the diffraction patterns taken from the GaN epilayer in Fig. 1, which correspond to the zb phase and show no evidence of large wz-GaN inclusions, and the XRD measurements which indicate a phase purity of at least 85%. We would not expect any small wz-GaN inclusions to influence the luminescence of the epilayer as any photogenerated carriers would be swept out of the inclusions due to internal fields in the crystal.

PL decay curves at 10 K of the HEB are monoexponential and the lifetimes increase from 0.15 ns to 0.67 ns with decreasing emission energy, as shown in Fig. 5. This is similar to behaviour previously observed for the HEB in other samples.[20]

### B. Modelling of SFs

A notable feature of the PL spectrum is the large width of the HEB. Since the TEM indicates the presence of a high density of SFs in the epilayers, a model of the unstrained band alignment between SFs and zb-GaN was investigated to demonstrate how the recombination of carriers confined at

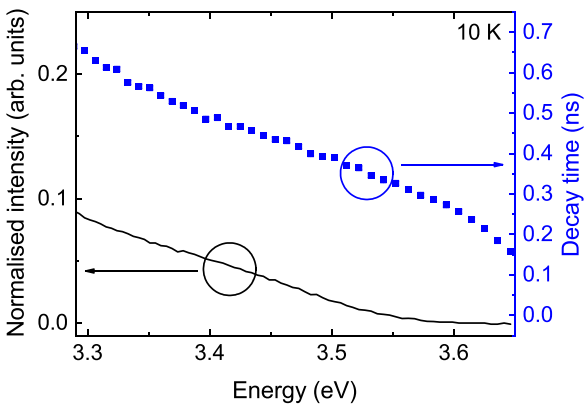


FIG. 5. PL lifetimes as a function of emission energy in the region of the HEB at 10 K with an excitation wavelength of 267 nm. Also shown for reference is a time-integrated PL spectrum obtained under the same conditions.

SFs can explain the width of the HEB. A study of zb-GaN embedded within wz-GaN nanowires[34] has shown how a broad emission band may result from such heterostructures due to contributions from structures with a variety of thicknesses. It is possible that in this sample a similar effect may occur due to different SF separations.

To investigate this, the conduction and valence band alignments were calculated in a bunch of identically spaced SFs, each treated as a 3 monolayer thick (equal to 0.78 nm) layer of wz-GaN, using the method discussed in our previous work.[20] In this model, a type II band alignment is assumed, with band offsets of 270 meV and 70 meV for the conduction and valence bands.[35] The spontaneous polarisation of the wz-GaN differs from the zb-GaN, as detailed in Table I: the change in polarisation at the SF interface therefore results in electric fields in both the zb- and wz-GaN as illustrated in Fig. 6.

We extend this approach by solving the time independent Schrödinger equation (TISE) in this structure for electrons and holes, with the boundary condition that the wavefunction must be zero at either side of the bunch. The Coulomb interaction between these carriers was modelled as follows: the hole wavefunction, $\psi_h$, and the hole energy were assumed to be unperturbed due to the larger hole effective mass and were therefore obtained by solving the TISE in a one-dimensional unperturbed potential. In the two in-plane directions, the potential was uniform; therefore, an exponentially decaying form for $\psi_h$ was chosen with a characteristic in-plane extent of $\lambda_h$.[35] An associated positive charge distribution in 3-dimensions, $p(\underline{\mathbf{r}})$, was calculated using the following equation:

$$p(\underline{\mathbf{r}}) = e\frac{|\psi_h|^2 \exp\left(\frac{-|r|}{\lambda_h}\right)}{\int |\psi_h|^2 \exp\left(\frac{-|r|}{\lambda_h}\right) d\underline{\mathbf{r}}}, \tag{1}$$

where $r$ is the in-plane distance and $e$ is the electron charge.

The charge distribution $p(\underline{\mathbf{r}})$ was used to modify the potential experienced by electrons at each point in a 3 dimensional space by an amount given by the following equation:

$$V_i(\underline{\mathbf{r}}) = \frac{-1}{4\pi\epsilon\epsilon_0}\int \frac{p(\underline{\mathbf{r_i}})}{|\underline{\mathbf{r_i}}|} d\underline{\mathbf{r_i}}. \tag{2}$$

To simplify the problem, the electron wavefunction was also assumed to decay exponentially in the plane, with an in-plane extent of $\lambda_e$, which is related to $\lambda_h$ in the following equation:

$$m_e\lambda_e = m_h\lambda_h. \tag{3}$$

A value for $\lambda_h$ of 0.4 nm was used in the model, as this results in a combined electron-hole in-plane wavefunction extent of 4.4 nm, which is a midrange value taken from modelling work performed previously on SFs in wz-GaN.[35] At each point along the direction of interest, a weighted mean was performed across all points in the plane, using the squared in-plane electron wavefunction as the weights. This enabled an effective one dimensional potential to be calculated, taking into account the impact of the Coulomb interaction in three dimensions. The one dimensional TISE was then solved in this effective potential to calculate the electron wavefunctions and energies. The electron-hole energy was then calculated as the difference between the energy of the electron and the hole. The impact of the Coulomb interaction on the recombination energy was calculated by solving the TISE whilst ignoring the effect of the Coulomb interaction, and calculating the energy difference between the solution with and without Coulomb effects.

This model is similar to that developed by Corfdir and Lefebvre,[35] which describes emission from SFs within wz-GaN: the key difference between them is in the nature of the QW-like regions. In the model of Corfdir and Lefebvre, the SF consists of zb-GaN which acts as a QW to confine the electron wavefunction. The hole is then bound to the electron

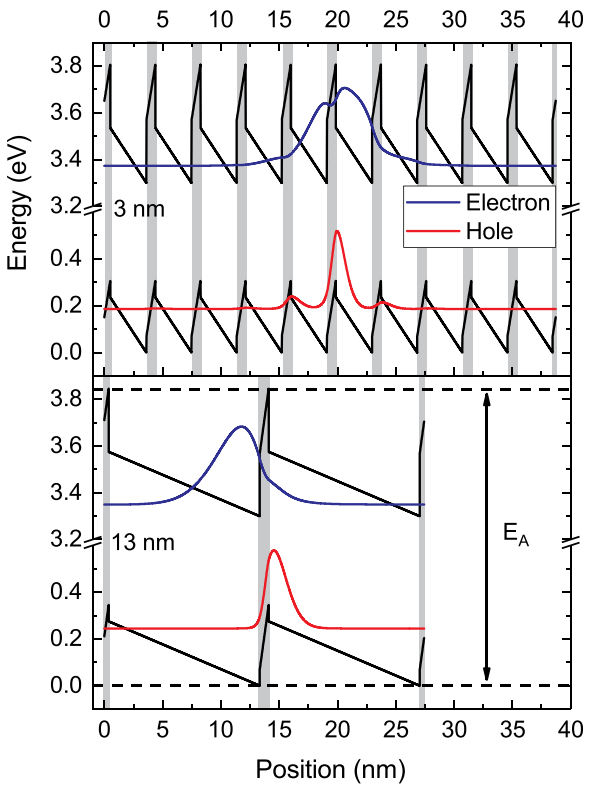


FIG. 6. Wavefunction solutions to the TISE in a bunch of SFs separated by 3 nm (top) and 13 nm (bottom) for one electron (blue) and one hole (red), accounting for the Coulomb interaction between the carriers. The SFs are highlighted by a light grey background.

TABLE I. Band parameters for zb and wz-GaN used for modelling. All values are taken from Ref. 30 unless otherwise specified. The hole effective mass lies within the spread of experimental results presented in Ref. 30. The effective masses of electrons and holes have been assumed to be the same in zb and wz-GaN for simplicity.

| | zb-GaN | wz-GaN |
|---|---|---|
| $E_g$ (eV) | 3.3 | 3.5 |
| $m_h^*(m_0)$ | 2 | 2 |
| $m_e^*(m_0)$ | 0.2 | 0.2 |
| $\epsilon$ | 9.7[21] | 10.28[36] |
| $P_{sp}$ (C m$^{-2}$) | 0 | −0.034 |

via the Coulomb interaction. The electron-hole energy is largely independent of the SF separation since the QW-width is unaffected. In our model, the SFs consist of wz-GaN, which act as barriers for the electrons. The electrons are hence confined to the zb-GaN which acts as a QW. The SF separation therefore directly impacts the width of the QW for the electrons which, when combined with strong electric fields such as in Fig. 6, can result in a variety of electron-hole energies.

The discussed model was implemented to calculate the electron-hole energies and Coulomb terms for a range of SF separations, which are shown in Fig. 7. To conserve computational power, the number of SFs within the bunch was scaled to suit the spread of the wavefunctions, whilst ensuring that there was minimal impact upon the calculated wavefunctions and energies. A bunch size of 2 SFs was used for SF separations above 5 nm, increasing to a maximum of 10 SFs for a SF separation of 1.5 nm. The full list of the parameter values used is given in Table I.

For SF separations less than 1.5 nm, neither the electron nor the hole is confined by the entire SF bunch. The carriers are not expected to influence the PL spectrum due to the lack of confinement; therefore, these results have been omitted from Fig. 7. For separations above 1.5 nm, the hole is confined within a triangular QW-like potential, as shown in Fig. 6. For closely packed SFs with separations less than 3 nm, the hole wavefunction, and positive charge distribution, spreads across several SFs, as shown on the top of Fig. 6. In this regime, the electron is confined to the bunch solely due to the Coulomb interaction and the electron wavefunction is spread across several QW-like zb regions.

As SF separation is increased up to 3 nm, the hole wavefunction becomes confined to a single SF, thereby dramatically increasing the positive charge density, leading to an increase in the Coulomb term from 49 meV to 82 meV, as seen in Fig. 7. This results in a rapid drop in the electron-hole energy. For SF separations above 3 nm, electrons are confined within one region of zb-GaN by a combination of the Coulomb attraction and the polarisation field. A solution to the TISE in this regime is shown on the bottom of Fig. 6. The Coulomb term slowly reduces at larger separations, due to the increasing separation between electrons and holes, and trends towards a value of 26 meV, which is the bulk value observed experimentally.[17]

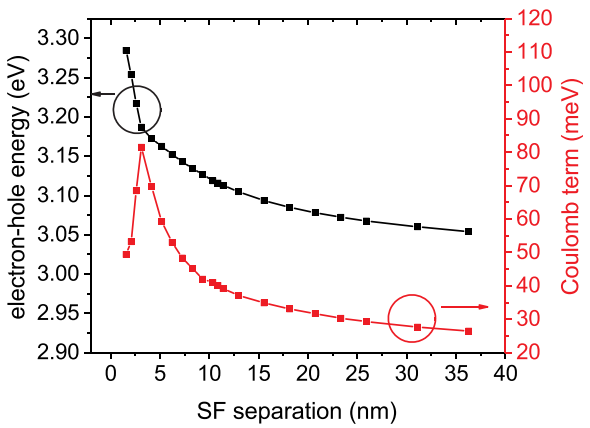


FIG. 7. The calculated electron-hole energies with varying SF separation for SF bunches with equally spaced SFs (black). The Coulomb interaction term, which is equal to the energy difference between solutions to the TISE with and without the Coulomb interaction.

The electron-hole energy varies by 230 meV over the range of SF separations, as shown in Fig. 7, which is large enough to account for the width of HEB in Fig. 3. A portion of this variation is caused by the Coulomb term, which varies by 56 meV. Additional variation is caused by the polarisation field, which separates the electrons and holes, causing a reduction of the energies as the separation increases. The reduction in confinement energy is also accompanied by a reduction in electron-hole wavefunction overlap due to this increasing separation.

During the PLE experiment, if a photon is absorbed with energy greater than the absorption edge then an electron-hole pair is created in the continuum of unconfined states. The carriers are captured into the potential wells shown in Fig. 6, subsequently cool to the ground states, and recombine. If the photon energy is reduced below $E_A$, as indicated in Fig. 6, absorption no longer occurs into the continuum of states. Instead, absorption occurs into the confined states with a reduced joint density of states when compared with the continuum: this effect reduces the strength of the absorption, leading to an absorption edge in the PLE spectrum. Figure 6 shows that this occurs for energies below around 3.8 eV, which corresponds with the HEB absorption edge in Fig. 4.

The model can also explain the variation of carrier lifetime with the recombination energy in Fig. 5. Electrons and holes confined within more closely packed SFs have a larger wavefunction overlap, and therefore a reduced radiative lifetime. Since Fig. 7 indicates that more closely packed SFs result in larger energy differences, the implication is that larger recombination energies will occur with shorter lifetimes, which agrees with the measurements in Fig. 5.

Reports in the literature disagree on the nature of the band alignment, some suggesting it as type II[37–39] and others as type I,[40–42] with a variety of band offset values. The model results were recalculated over the range of band offsets reported, for each type of band alignment, resulting in a maximum electron-hole energy change of the order of 20 meV. This causes no appreciable change in the variation of electron-hole energy with SF separation as shown in Fig. 7.

Although the model can explain why SF-emission results in a broadband in the PL spectrum, the calculated electron-hole energies in Fig. 7 do not correspond directly to the emission energies in Fig. 3, and do not extend above the bandgap of zb-GaN. This can be explained as follows: a sufficient number of SFs were included in each calculation to ensure that the electron wavefunction was confined by the microstructure modelled and not by the finite thickness of the epilayer used in each calculation. The alternative approach of significantly increasing the modelled epilayer thickness both greatly extends the time required for calculations and reduces the accuracy of the resulting wavefunction.[43] For the smallest SF separation, this approach resulted in up to 10 SFs being included, effectively forming a superlattice, which has been shown to reduce transition energies compared to isolated QWs in similar AlGaAs structures.[44]

However, in TEM measurements, isolated structures of 2 SFs can be found. An estimate for the maximum emission energy of such structures, obtained via inspection of the band alignment for the 1.5 nm separated SF system, is 3.75 eV, significantly in excess of the bandgap of zb-GaN. We therefore attribute the emission above the zb-GaN bandgap to these lone pairs of SFs.

It has been observed previously in TEM measurements that the density of SFs reduces with increasing epilayer thickness due to annihilation of SFs on different {111} crystal facets.[12,23] The model would therefore predict that the intensity of the HEB would reduce as the epilayer thickness is increased: this is an avenue which requires further investigation.

## IV. CONCLUSION

The luminescence properties are presented of an MOCVD-grown zb-GaN epilayer. This revealed the presence of $D^0X$ and DAP emission, along with an HEB with a peak at 3.4 eV and FWHM of 200 meV, extending above the bandgap of zb and wz-GaN. The HEB corresponds to a broad absorption edge centred at 3.6 eV and has fast monoexponential time decays which become slower at lower recombination energies.

TEM measurements show no evidence of wz-GaN inclusions which are typically used to explain emission at these energies. However, bunches of SFs can be used to account for this emission band. A band alignment model for the interfaces between the zb-GaN and the SFs showed that differently spaced SFs result in a dramatic change in the electrons-hole energy and hence can explain the width of the HEB.

## ACKNOWLEDGMENTS

This was work funded by EPSRC under Grant Nos. EP/M010627/1 and EP/N01202X/1, and Innovate UK under Grant No. 56917-383420. Additional research data supporting this publication are available from the University of Manchester repository at 10.15127/1.304093.

[1]N. Bardsley, S. Bland, L. Hansen, M. Pattison, M. Pattison, K. Stober, and M. Yamada, *US Department of Energy 2015 Solid-State Lighting RD Plan* (US Department of Energy, 2015).
[2]K. A. Bulashevich, A. V. Kulik, and S. Y. Karpov, Phys. Status Solidi (a) **212**, 914 (2015).
[3]M. Feneberg, F. Lipski, R. Sauer, K. Thonke, T. Wunderer, B. Neubert, P. Bruckner, and F. Scholz, Appl. Phys. Lett. **89**, 242112 (2006).
[4]B. A. Haskell, F. Wu, M. D. Craven, S. Matsuda, P. T. Fini, T. Fujii, K. Fujito, S. P. DenBaars, J. S. Speck, and S. Nakamura, Appl. Phys. Lett. **83**, 644 (2003).
[5]P. P. Paskov, R. Schifano, B. Monemar, T. Paskova, S. Figge, and D. Hommel, J. Appl. Phys. **98**, 093519 (2005).
[6]P. Corfdir, P. Lefebvre, J. Levrat, A. Dussaigne, J.-D. Ganiere, D. Martin, J. Ristic, T. Zhu, N. Grandjean, and B. Deveaud-Pledran, J. Appl. Phys. **105**, 043102 (2009).
[7]M. J. Davies, P. Dawson, S. Hammersley, T. Zhu, M. J. Kappers, C. J. Humphreys, and R. A. Oliver, Appl. Phys. Lett. **108**, 252101 (2016).
[8]S. C. Ling, T. C. Lu, S. P. Chang, J. R. Chen, H. C. Kuo, and S. C. Wang, Appl. Phys. Lett. **96**, 231101 (2010).
[9]K. Nishizuka, M. Funato, Y. Kawakami, S. Fujita, Y. Narukawa, and T. Mukai, Appl. Phys. Lett. **85**, 3122 (2004).
[10]H.-H. Huang and Y.-R. Wu, J. Appl. Phys. **107**, 053112 (2010).
[11]D. J. As, Microelectron. J. **40**, 204 (2009).
[12]B. Daudin, G. Feuillet, J. Hubner, Y. Samson, F. Widmann, A. Philippe, C. Bru-Chevallier, G. Guillot, E. Bustarret, G. Bentoumi, and A. Deneuville, J. Appl. Phys. **84**, 2295 (1998).
[13]D. Wang, Y. Hiroyama, M. Tamura, M. Ichikawa, and S. Yoshida, J. Cryst. Growth **220**, 204 (2000).
[14]E. Martinez-Guerrero, B. Daudin, G. Feuillet, H. Mariette, Y. Genuist, S. Fanget, A. Philippe, C. Dubois, C. Bru-Chevallier, G. Guillot, P. Aboughe Nze, T. Chassagne, Y. Monteil, H. Gamez-Cuatzin, and J. Tardy, Mater. Sci. Eng. B **82**, 59 (2001).
[15]C. H. Wei, Z. Y. Xie, L. Y. Li, Q. M. Yu, and J. H. Edgar, J. Electron. Mater. **29**, 317 (2000).
[16]G. Feuillet, F. Widmann, B. Daudin, J. Schuler, M. Arlery, J. L. Rouvière, N. Pelekanos, and O. Briot, Mater. Sci. Eng. B **50**, 233 (1997).
[17]M. Feneberg, M. Röppischer, C. Cobet, N. Esser, J. Schörmann, T. Schupp, D. J. As, F. Hörich, J. Bläsing, A. Krost, and R. Goldhahn, Phys. Rev. B **85**, 155207 (2012).
[18]A. Philippe, C. Bru-Chevallier, M. Vernay, G. Guillot, J. Hü Bner, B. Daudin, and G. Feuillet, Mater. Sci. Eng. B **59**, 168 (1999).
[19]R. M. Kemper, D. J. As, and J. K. N. Lindner, "Cubic GaN on nanopatterned 3c-sic/si (001) substrates," in *Silicon-Based Nanomaterials*, edited by H. Li, J. Wu, and Z. M. Wang (Springer, New York, NY, 2013), pp. 381–405.
[20]S. A. Church, S. Hammersley, P. W. Mitchell, M. J. Kappers, S. L. Sahonta, M. Frentrup, D. Nilsson, P. J. Ward, L. J. Shaw, D. J. Wallis, C. J. Humphreys, R. A. Oliver, D. J. Binks, and P. Dawson, Phys. Status Solidi (b) **254**, 1600733 (2017).
[21]V. Bougrov, M. E. Levinshtein, S. L. Rumyantsev, and A. Zubrilov, *Properties of Advanced Semiconductor Materials GaN, AlN, InN, BN, SiC, SiGe* (John Wiley & Sons Inc., 2001), pp. 1–30.
[22]R. M. Kemper, P. Veit, C. Mietze, A. Dempewolf, T. Wecker, F. Bertram, J. Christen, J. K. N. Lindner, and D. J. As, Phys. Status Solidi (c) **12**, 469 (2015).
[23]M. Rüsing, T. Wecker, G. Berth, D. J. As, and A. Zrenner, Phys. Status Solidi (b) **253**, 778–782 (2016).
[24]S. Waheeda, N. Zainal, Z. Hassan, S. Novikov, A. Akimov, and A. Kent, Appl. Surf. Sci. **317**, 1010 (2014).
[25]H. Okumura, K. Ohta, G. Feuillet, K. Balakrishnan, S. Chichibu, H. Hamaguchi, P. Hacke, and S. Yoshida, J. Cryst. Growth **178**, 113 (1997).
[26]M. Frentrup, L. Y. Lee, S-l. Sahonta, M. J. Kappers, F. Massabuau, P. Gupta, R. A. Oliver, C. J. Humphreys, and D. J. Wallis, J. Phys. D: Appl. Phys. **50**, 433002 (2017).
[27]D. J. As, D. Schikora, and K. Lischka, Phys. Status Solidi (c) **0**, 1607 (2003).
[28]M. J. Paisley, Z. Sitar, J. B. Posthill, and R. F. Davis, J. Vac. Sci. Technol. A Vac., Surf., Films **7**, 701 (1989).
[29]A. Nakadaira and H. Tanaka, J. Electron. Mater. **26**, 320 (1997).
[30]I. Vurgaftman and J. R. Meyer, J. Appl. Phys. **94**, 3675 (2003).
[31]J. Wu, H. Yaguchi, K. Onabe, R. Ito, and Y. Shiraki, Appl. Phys. Lett. **71**, 2067 (1997).
[32]D. Xu, H. Yang, J. B. Li, D. G. Zhao, S. F. Li, S. M. Zhuang, R. H. Wu, Y. Chen, and G. H. Li, Appl. Phys. Lett. **76**, 3025 (2000).
[33]J. F. Muth, J. H. Lee, I. K. Shmagin, R. M. Kolbas, H. C. Casey, B. P. Keller, U. K. Mishra, and S. P. DenBaars, Appl. Phys. Lett. **71**, 2572 (1997).
[34]G. Jacopin, L. Rigutti, L. Largeau, F. Fortuna, F. Furtmayr, F. H. Julien, M. Eickhoff, and M. Tchernycheva, J. Appl. Phys. **110**, 064313 (2011).
[35]P. Corfdir and P. Lefebvre, J. Appl. Phys. **112**, 053512 (2012).
[36]F. Bernardini, V. Fiorentini, and D. Vanderbilt, Phys. Rev. Lett. **79**, 3958 (1997).
[37]M. Murayama and T. Nakayama, Phys. Rev. B **49**, 4710 (1994).
[38]Y. T. Rebane, Y. G. Shreter, and M. Albrecht, Phys. Status Solidi (a) **164**, 141 (1997).
[39]C. Stampfl and C. G. Van de Walle, Phys. Rev. B **57**, R15052 (1998).
[40]C.-Y. Yeh, S.-H. Wei, and A. Zunger, Phys. Rev. B **50**, 2715 (1994).
[41]J. A. Majewski and P. Vogl, Internet J. Nitride Semicond. Res. **3**, 21 (1998).
[42]A. Belabbes, L. C. de Carvalho, A. Schleife, and F. Bechstedt, Phys. Rev. B **84**, 125108 (2011).
[43]P. Harrison, *Quantum Wells, Wires and Dots* (John Wiley & Sons, Ltd, 2006), Chap. 3.3, pp. 72–75.
[44]P. Harrison, *Quantum Wells, Wires and Dots* (John Wiley & Sons, Ltd, 2006) Chap. 16.2, pp. 471–474.